



Photosynthetically active radiation from Clouds and the Earth's Radiant Energy System (CERES) products

Wenyong Su,^{1,2} Thomas P. Charlock,³ Fred G. Rose,⁴ and David Rutan⁴

Received 15 August 2006; revised 1 February 2007; accepted 26 February 2007; published 16 May 2007.

[1] We describe a method that retrieves surface photosynthetically active radiation (PAR) and its direct and diffuse components from the Surface and Atmospheric Radiation Budget (SARB) product of Clouds and the Earth's Radiant Energy System (CERES). The shortwave spectrum in the SARB Edition 2 is calculated in 15 bands, 4 of which are used to develop the PAR, in conjunction with the look-up tables described in this paper. We apply these look-up tables to existing CERES Terra Edition 2 products. The new retrieved surface PAR is validated with LI-COR PAR measurements at seven Surface Radiation Budget Network (SURFRAD) sites using data from March 2000 to June 2005. The relative bias of retrieved all-sky PAR at the SURFRAD sites is 4.6% (positive sign indicating retrieval exceeds measurement), and 54% of the all-sky samples are within the $\pm 10\%$ uncertainty of the LI-COR PAR measurements. The satellite field-of-view (FOV) is more representative of the ground instrument FOV under clear conditions, so 89% of clear-sky retrievals are within the uncertainty of the LI-COR PAR measurements at SURFRAD sites with positive biases at most sites. The retrieved PAR is also validated at the Atmospheric Radiation Measurement (ARM) Southern Great Plains Central Facility (CF) site using data from October 2003 to June 2004 for those FOVs having both LI-COR and Rotating Shadowband Spectroradiometer (RSS) ground measurements; for this small domain, all-sky relative biases are again positive (1.9%) for LI-COR but negative (-4.2%) for RSS. The direct-to-diffuse ratio derived from CERES is smaller than that from RSS for both clear and cloudy conditions. CERES also retrieves the broadband shortwave insolation, and the relative biases for the broadband retrievals are much less than those for PAR at the above sites. It appears that some of the ground-based measurements of PAR do not have the fidelity of those for broadband shortwave insolation.

Citation: Su, W., T. P. Charlock, F. G. Rose, and D. Rutan (2007), Photosynthetically active radiation from Clouds and the Earth's Radiant Energy System (CERES) products, *J. Geophys. Res.*, 112, G02022, doi:10.1029/2006JG000290.

1. Introduction

[2] Nearly all living things depend on energy produced from photosynthesis for their nourishment, making photosynthesis vital to life on Earth. In the photosynthesis process, radiative energy from sunlight is converted to chemical energy by using CO_2 from the atmosphere. Solar energy in the spectrum of 400–700 nm, the so-called photosynthetically active radiation (PAR), plays a very important role in photosynthesis. The intensity of PAR affects the rate of photosynthesis, and hence also the carbon sequestration by ecosystems. Therefore PAR is a key variable for modeling global gross and net primary produc-

tion. This study defines PAR as the downwelling solar irradiance from 400–700 nm at the surface.

[3] Surface PAR has been calculated from satellite measurements. *Eck and Dye* [1991] estimated monthly mean surface PAR from Total Ozone Mapping Spectrometer (TOMS), which typically takes one measurement per day at a spatial resolution of 500 km. They first calculated clear sky surface PAR from a parameterization accounting for ozone absorption, Rayleigh scattering, and aerosol scattering. A constant total column ozone of 300 Dobson Unit (DU) and a constant aerosol optical depth of 0.2 were assumed for all locations and months. They then used radiance from the 370 nm channel on TOMS to correct the effects of clouds on surface PAR, assuming clouds are nonabsorbing and their reflectivity is constant across ultraviolet (UV) and PAR spectrum.

[4] *Bishop and Rossow* [1991] calculated daily surface broadband solar flux for the globe using cloud optical properties derived from 3-hourly International Satellite Cloud Climatology Project (ISCCP) C1 data. *Potter et al.* [1993] then simply applied an adjustment factor of 0.5 to this solar flux to derive surface PAR (this product is referred

¹Department of Atmospheric and Planetary Sciences, Hampton University, Hampton, Virginia, USA.

²Now at Science Systems and Applications, Inc., Hampton, Virginia, USA.

³NASA Langley Research Center, Hampton, Virginia, USA.

⁴Science Systems and Applications, Inc., Hampton, Virginia, USA.

to as ISCCP-P). The needs of the biological community have motivated the development of more PAR retrievals. *Pinker and Laszlo* [1992a] computed PAR with ISCCP C1 data based on a model originally developed for broadband surface flux (0.2–4.0 μm) [*Pinker and Ewing*, 1985; *Pinker and Laszlo*, 1992b]. Their model uses the relationship between broadband atmospheric transmissivity T and top of atmosphere broadband reflectivity R from radiative transfer calculations. By matching the model-derived R , as it pertains to a given atmospheric and surface condition, to R observed by the satellite, one can determine the corresponding T , and therefore the surface broadband flux. They divided the broadband into five spectral intervals: 0.2–0.4 μm , 0.4–0.5 μm , 0.5–0.6 μm , 0.6–0.7 μm , and 0.7–4.0 μm . PAR is obtained simply by summing the spectral fluxes in the 0.4–0.5 μm , 0.5–0.6 μm , and 0.6–0.7 μm intervals. The algorithm was applied to ISCCP C1 data at a 250 km resolution and produced the first global map of monthly PAR (this product is referred to as ISCCP-PL). Global Energy and Water Cycle Experiment's (GEWEX) Surface Radiative Budget (SRB) project also applies a modified version of this algorithm to ISCCP DX data and produces PAR at a spatial resolution of 1 degree.

[5] PAR over the ocean was also produced by the Sea-viewing Wide Field-of-view Sensor (SeaWiFS) [*Frouin et al.*, 2003]. SeaWiFS views most of the ocean once a day. The SeaWiFS PAR algorithm used plane-parallel theory and assumed that the effect of clouds could be decoupled from the clear atmosphere. SeaWiFS radiances between 412 and 670 nm were used to derive an approximate cloud-surface system albedo for the 400- to 700-nm interval and then produce daily averaged surface PAR over the ocean.

[6] The Moderate Resolution Imaging Spectroradiometer (MODIS) team retrieved the fraction of the incident PAR absorbed by vegetation, but not PAR itself. The MODIS net primary production algorithm relies on the three-hourly, 1° by 1.25° spatial resolution PAR product assimilated at the NASA Global Modeling and Assimilation Office [*Running et al.*, 2004], though the algorithm itself has a resolution of 1 km. Therefore a high-resolution PAR product is urgently needed, especially over land.

[7] Recent studies of photosynthesis highlight the importance of the diffuse component of PAR, as well as total PAR [*Cohan et al.*, 2002; *Gu et al.*, 1999, 2002; *Niyogi et al.*, 2004]. A higher diffuse portion of PAR has been associated with a higher rate of forest net ecosystem exchange of CO_2 [*Price and Black*, 1990; *Hollinger et al.*, 1994; *Fan et al.*, 1995; *Goulden et al.*, 1997]. The study of *Gu et al.* [2002] using field data pointed out the need to provide diffuse PAR in addition to total PAR. However, none of the satellite data sets mentioned earlier provide separate direct and diffuse components of PAR, except the GEWEX SRB product.

[8] Prior to the mid 1990s, surface PAR measurements were rare [*Bishop et al.*, 1997]. Therefore it was nearly impossible to fully validate the satellite-based PAR retrievals. *Eck and Dye* [1991] used pyranometers to validate their PAR, simply by multiplying 0.48 to convert the pyranometer measured flux to PAR. Comparisons were done for three sites. The relative difference between monthly mean PAR from TOMS and that estimated from pyranometers was less than 6%. *Dye and Shibasaki* [1995] compared three PAR retrievals with ground PAR measurements at Moscow.

The comparison indicated that for snow/ice-free months (April to October, 1987), the RMS errors were 28.1%, 13.7%, and 7.2% for ISCCP-P, ISCCP-PL, and TOMS PAR respectively. However, as pointed out by *Dye and Shibasaki* [1995], such a single site comparison does not represent the overall quality of the data sets. They stressed the need to establish long-term, global network of ground-based PAR sensors to validate and refine different PAR data sets.

[9] PAR is measured at many observational networks now, such as Surface Radiation Budget Network (SURFRAD) [*Augustine et al.*, 2000], U.S. Department of Agriculture (USDA) UV network [*Bigelow et al.*, 1998], and FLUXNET network [*Baldocchi et al.*, 2001]. These networks use the LI-COR quantum sensor which has an interference filter to measure flux in the spectral range of 0.4 to 0.7 μm . The sensor essentially counts the number of photons with equal weight, regardless of wavelength within the band. The estimated uncertainty of the measurement for PAR is about $\pm 10\%$ (*J. Augustine*, personal communication, 2006). One alternative is the Rotating Shadowband Spectroradiometer (RSS). The RSS provides continuous spectral measurements of total-horizontal, diffuse-horizontal, and direct-normal fluxes in over 1000 distinct channels from 0.36 to 1.05 μm [*Harrison et al.*, 1999] and has been deployed at Atmospheric Radiation Measurement (ARM) Southern Great Plains (SGP) Central Facility (CF) since May of 2003. Its uncertainty was estimated to be better than $\pm 4\%$ [*Kiedron et al.*, 1999; *Harrison et al.*, 2003]. Routine RSS measurements are available only at ARM SGP CF (one site). It is the only publicly available data source with a substantial record, that we have found, which suffices to validate both direct and diffuse PAR retrieved with Terra.

[10] The PAR algorithm described here uses aerosol and cloud input data from the Earth Observing System (EOS). The new algorithm generates surface PAR by adjusting spectral fluxes contained in the Surface and Atmospheric Radiation Budget (SARB) component of the Clouds and the Earth's Radiant Energy System (CERES). An algorithm for surface UV [*Su et al.*, 2005] uses the same resource. While mainly intended to provide observations of broadband TOA fluxes, CERES [*Wielicki et al.*, 1996] includes a program to compute the fluxes at TOA, within the atmosphere and at the surface, and also to validate with independent ground-based measurements [*Charlock and Alberta*, 1996]. SARB is based on fairly detailed retrievals of aerosol and cloud optical properties, which are used to partition total PAR into direct and diffuse components. The SARB broadband shortwave (SW) is divided into 15 narrow bands, 4 of which we employ for our PAR calculation. The basic SARB calculation and its inputs are summarized in section 2. A high-resolution radiative transfer model is needed to adjust the spectral fluxes of the SARB bands, this is briefly described in section 3. Methods of deriving surface PAR from SARB and decomposing it into direct and diffuse PAR are presented in section 4. Validations of surface PAR and the ratio of direct to diffuse PAR are given in section 5.

2. CERES Surface and Atmospheric Radiation Budget Calculation

[11] The CERES instrument measures radiances in three channels: a broadband shortwave channel (0.3–5 μm), a

window channel (8–12 μm), and a total channel (0.3–100 μm). The CERES radiances are converted to reflected shortwave (SW), emitted longwave (LW), and emitted window (WN) TOA fluxes. The large CERES footprints (~ 20 – 40 km) of the TRMM satellite are matched with smaller Visible Infrared Scanner (VIRS) pixels, and the large CERES footprints of the Terra and Aqua satellites are matched with smaller Moderate Resolution Imaging Spectroradiometer (MODIS) pixels. The SARB product [Charlock *et al.*, 2006] provides vertical profiles of SW, LW, and WN channels at the TOA, 70 hPa, 200 hPa, 500 hPa, and the surface using a fast, plane parallel correlated- k radiative transfer code [Fu and Liou, 1992, 1993], which has been highly modified and now dubbed the “Langley Fu-Liou code” [Rose and Charlock, 2002]. The HITRAN2000 database was used for the determination of correlated- k 's in the SW [Kato *et al.*, 1999]. We make a first-order accounting for inhomogeneous cloud optical thickness by using the gamma weighted two stream approximation in the SW [Kato *et al.*, 2005]. An external mixture of aerosols, clouds, and gases is assumed. All-sky aerosol forcing is determined by running with clouds (if present), gases, and aerosols, and subtracting the flux from a run with no aerosols. A theoretical clear-sky aerosol forcing is computed for all footprints as the difference of the cloud-free flux with aerosols minus the cloud-free flux with no aerosols.

[12] Cloud properties are the most critical inputs for the calculation. We use retrievals of cloud optical depth, cloud phase (liquid or ice), effective droplet radius or ice crystal diameter, liquid water path or ice water path, and effective radiating temperature (with estimates of cloud top pressure and geometrical thickness) generated by the CERES team [Minnis *et al.*, 2002]. They are based on imager data (VIRS on TRMM, MODIS on Terra and Aqua, and ISCCP B1 geostationary radiances; see Rossow and Schiffer [1991] for ISCCP) and assume plane-parallel, and single-layered clouds [Minnis *et al.*, 2002]. All of the various imager pixels have higher spatial resolution than the coarse footprints of the broadband CERES instrument. The daytime retrieval technique [Arduini *et al.*, 2002] provides optical depth from a visible channel over snow-free areas, and the daytime snow retrieval technique [Platnick *et al.*, 2001] provides optical depth from a near infrared channel over snow-covered areas.

[13] Aerosol optical depth (AOD) retrievals are based on VIRS [Ignatov and Stowe, 2000] when processing CERES TRMM data, and are based on MODIS [Kaufman *et al.*, 1997] when processing CERES Terra and Aqua data. Over the ocean, MOD04 is used for 7 wavelengths; the AOD is interpolated to the remainder of the spectrum using the selected aerosol type, as specified below. Over the land, MOD04 provides AOD at 3 wavelengths, and the MOD04 Angstrom exponent is used to guide the extension over the spectrum. If the MOD04 instantaneous AOD is not available (i.e., footprint is overcast), we temporally interpolate from a file of the MODIS Daily Gridded Aerosol. When cloudiness in the footprint exceeds 50%, or when there is no MODIS AOD, we use AOD from the NCAR Model for Atmospheric Transport and Chemistry (MATCH) assimilation [Collins *et al.*, 2001]. When AOD is taken from MATCH, we assume it for one wavelength only (630 nm). MATCH AOD is apportioned to 7 types (small dust, large

dust, soot, soluble organic, insoluble organic, sulfate, and sea salt) on a daily basis over the globe for all-sky conditions. Aerosol type is always taken from MATCH and is used to determine the selection of the asymmetry factor (g) and the single scattering albedo (SSA). Asymmetry factors and SSA are taken from the *Tegen and Lacis* [1996], or the Optical Properties of Aerosols and Clouds (OPAC) model [Hess *et al.*, 1998].

[14] Calculations are done for roughly 60,000,000 FOVs per month. Land surface albedos are retrieved for clear FOVs by matching a look-up table (LUT) for the 2-stream code to CERES broadband observations of SW flux at TOA [Rutan *et al.*, 2006]. The relative spectral shape of the surface albedo (but not the broadband solution from the LUT) is specified according to the CERES surface property maps, which are keyed to International Geophysical Bi-spherical Project (IGBP) land types. The spectral shapes of sea ice and snow are assumed from theoretical calculations [Jin and Stamnes, 1994]. For each location, a monthly archive of broadband land surface albedo is obtained for the most favorable, clear-sky viewing geometry. When cloudy during the month, this archived, clear-sky based surface albedo is then adjusted to account for the more diffuse field beneath the cloud. The spectral albedo of the ocean surface is obtained using a LUT considering SZA, wind speed, chlorophyll concentration, and cloud/aerosol optical depth [Jin *et al.*, 2004].

[15] We use daily global ozone profiles from Stratosphere Monitoring Ozone Blended Analysis (SMOBA) (S.-K. Yang *et al.*, SMOBA: A 3-dimensional daily ozone analysis using SBUV/2 and TOVS measurement, 1999, <http://www.cpc.ncep.noaa.gov/products/stratosphere/SMOBA/>). We use temperature and humidity profiles from ECMWF [Rabier *et al.*, 1998] for TRMM and from the Goddard Earth Observing System (GEOS-4) [Bloom *et al.*, 2005] for Terra and Aqua. Surface elevation is taken from the U.S. Geological Survey GTOPO30 digital elevation model.

[16] CERES PAR product is generated in two main formats: the instantaneous CERES broadband footprint (“CRS”) and the time-averaged grid box (“SYNI”). For the SYNI product, a complex algorithm [Young *et al.*, 1998; Rose *et al.*, 2006] combines and interpolates CERES measurements with geostationary results for hourly estimates of cloud properties and broadband TOA flux. Of the 24 hourly estimates of cloud properties in a SYNI grid box for one day, typically 8 will be from 3-hourly narrowband GOES geostationary retrievals, only 2 will be from MODIS or VIRS retrievals matched with CERES, and the remainder (typically 14 of 24) will be interpolated. At this writing, none of the SYNI products have been released. The archived Terra Edition 2B CRS and TRMM Edition 2C CRS products have a dated approximation to “PAR” as 437.5–689.7 nm. The correct PAR as 400–700 nm will be found on the forthcoming releases of Terra Edition 2 SYNI, Aqua Edition 2 CRS and SYNI, and all of Edition 3. All results presented in this paper are from the instantaneous footprint results of CERES on Terra and a SARB code with the correct PAR. Of the 15 SW bands in the Langley Fu-Liou code, band 7 (357.5–437.5 nm), band 8 (437.5–497.5 nm), band 9 (497.5–595.5 nm), and band 10 (595.5–689.7 nm) overlap the PAR spectral range. In this study, we focus on producing surface PAR and its direct and diffuse compo-

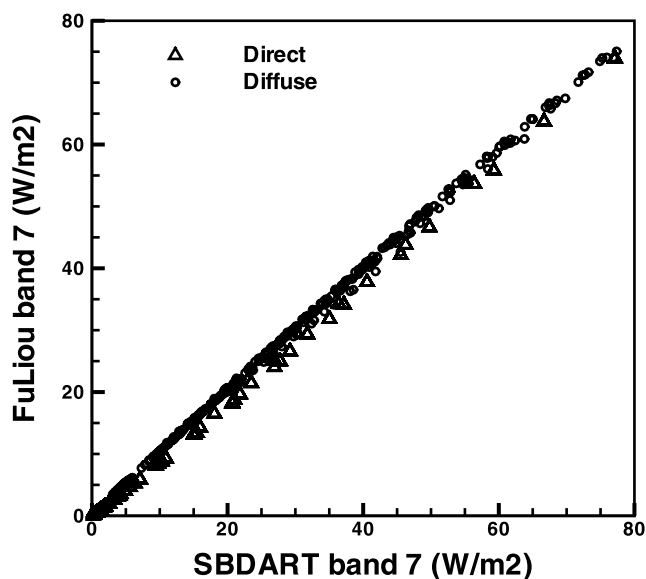


Figure 1. SBDART and SARB simulated direct (triangles) and diffuse (circles) fluxes for band 7.

nents using the outputs of bands 8 and 9 and adjustments to bands 7 and 10.

3. Radiative Transfer Simulation

[17] In order to provide accurate PAR at the surface, we must adjust the outputs of band 7 to cover 400–437.5 nm (hereafter referred to as adjusted band 7), and band 10 to cover 595.5–700 nm (hereafter referred to as adjusted band 10). The adjustments are done separately for direct and diffuse fluxes for band 7 and band 10. Here we define the adjustment factor γ_7^{dir} as the ratio of band 7 direct flux to

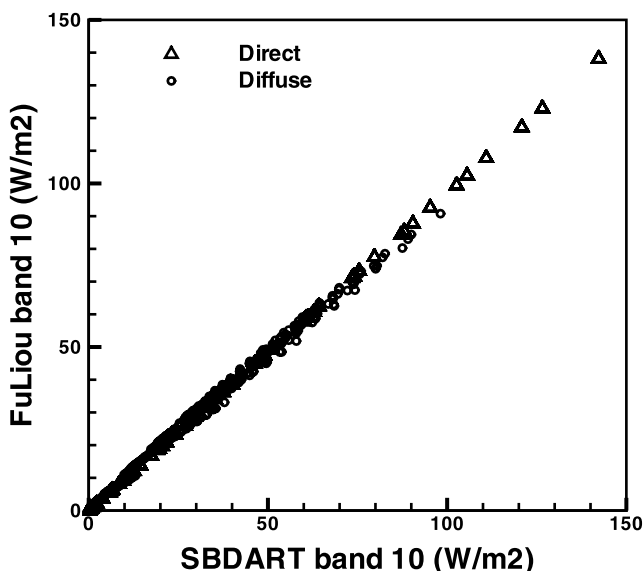


Figure 2. SBDART and SARB simulated direct (triangles) and diffuse (circles) fluxes for band 10.

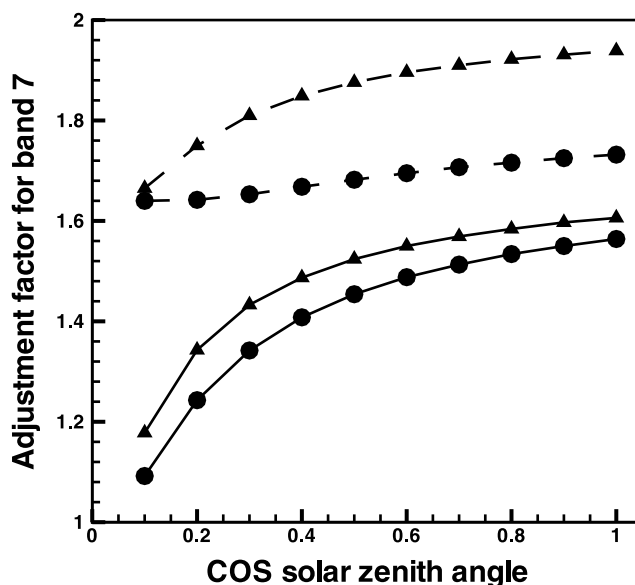


Figure 3. Adjustment factor γ_7^{dir} (solid lines) and γ_7^{dif} (dashed lines) as a function of cosine of SZA for continental average aerosols with optical depth of 0.02 (triangles) and 0.5 (circles). The simulation is for ocean surface and midlatitude summer atmosphere.

adjusted band 7 direct flux, and adjustment factor γ_7^{dif} as the ratio of band 7 diffuse flux to adjusted band 7 diffuse flux. Similarly, we define adjustment factor γ_{10}^{dir} as the ratio of band 10 direct flux to adjusted band 10 direct flux, and adjustment factor γ_{10}^{dif} as the ratio of band 10 diffuse flux to adjusted band 10 diffuse flux.

[18] We need a high-resolution atmospheric radiative transfer model to simulate fluxes of band 7, adjusted band 7, band 10, and adjusted band 10. Here we chose SBDART (Santa Barbara Discrete ordinate Atmospheric Radiative Transfer [see Ricchiazzi *et al.*, 1998]). Our goal is to use SBDART to calculate γ_7^{dir} , γ_7^{dif} , γ_{10}^{dir} and γ_{10}^{dif} , and thereby adjust the SARB output to provide surface PAR. Before we proceed further, we test the agreement between fluxes of band 7 and band 10 from SBDART and those from SARB output. We run SBDART and SARB for continental aerosols [d'Almeida *et al.*, 1991] for the following 360 cases: (1) cosine of solar zenith angle (SZA) from 0.1 to 1 in steps of 0.1; (2) aerosol optical depth (AOD) from 0.02 to 1.02 in steps of 0.2; and (3) surface albedo from 0.0 to 1.0 in steps of 0.2. Figure 1 shows the direct and diffuse fluxes of band 7 from SBDART and SARB agree very well, with RMS errors of 1.79 W/m² and 0.79 W/m², respectively; and the correlation coefficients are over 0.999. Figure 2 shows the results of band 10. The RMS errors are 1.75 W/m² and 1.91 W/m² for direct and diffuse fluxes, and the correlation coefficients are 0.999 and 0.998, respectively. Therefore we conclude that SBDART and SARB simulations are very close. Hereafter we use SBDART to calculate the direct and diffuse fluxes of band 7 and adjusted band 7, and the direct and diffuse fluxes of band 10 and adjusted band 10.

[19] The aerosol optical properties that we use in SBDART are from the OPAC package [Hess *et al.*, 1998]. The four types used are: maritime clean, continental aver-

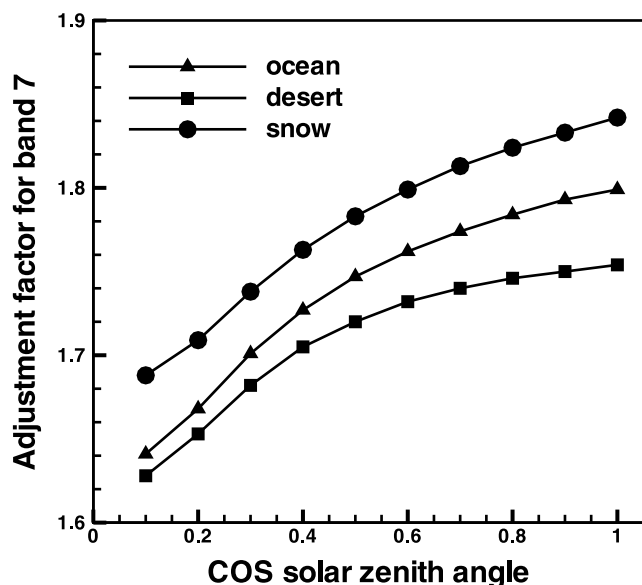


Figure 4. Adjustment factor γ_7^{dif} as a function of cosine of SZA for surface types of ocean, desert, and snow. Continental average aerosols with optical depth of 0.2 and midlatitude summer atmosphere were used here.

age, dust, and urban. Their single scattering albedos at 550 nm are: 0.97, 0.89, 0.88, and 0.76, encompassing both predominately scattering and strongly absorbing aerosols.

4. Deriving Surface PAR and Its Direct-to-Diffuse Ratio From SARB

[20] To provide adjustment factors γ_7^{dir} , γ_7^{dif} , γ_{10}^{dir} , and γ_{10}^{dif} for various conditions, we have done some sensitivity studies using SBDART. Results for γ_{10}^{dir} and γ_{10}^{dif} are the same as γ_7^{dir} and γ_7^{dif} , therefore we only present results of γ_7^{dir} and γ_7^{dif} here.

[21] For clear sky, we consider the effects of SZA, aerosol optical depth, aerosol type, surface albedo, precipitable water, surface elevation, and total column ozone on γ_7^{dir} and γ_7^{dif} . Figure 3 shows γ_7^{dir} (solid lines) and γ_7^{dif} (dashed lines) as a function of cosine of SZA for continental average aerosols with optical depth of 0.02 (triangles) and 0.5 (circles). The simulation is done for an ocean surface and a mid latitude summer atmosphere. Adjustment factors γ_7^{dir} and γ_7^{dif} are sensitive to SZA, and decrease as the sun approaches the horizon. For overhead sun, γ_7^{dir} and γ_7^{dif} change by about 3% and 12% when AOD increases from 0.02 to 0.5. Figure 4 shows γ_7^{dif} as a function of cosine of SZA for three surface types: ocean, desert, and snow. The surface albedo across the PAR spectrum ranges from 0.09 to 0.06 for the ocean, from 0.17 to 0.41 for the desert, and from 0.96 to 0.64 for the snow. We used continental average aerosols with optical depth of 0.2 in the simulation. At a given SZA, γ_7^{dif} for snow is about 4% larger than for ocean, and about 6% larger for snow than for desert. In contrast to γ_7^{dif} , the adjustment factor γ_7^{dir} is not sensitive to surface albedo (not shown). Figure 5 shows γ_7^{dir} (solid lines) and γ_7^{dif} (dashed lines) for continental average aerosols (triangles) and urban aerosols (circles), both with AOD of 0.2, and for an ocean surface. For any SZA, γ_7^{dir} and γ_7^{dif} change by only about 0.2% among the different aerosol

types. The adjustment factors γ_7^{dir} and γ_7^{dif} have negligible sensitivity to precipitable water, surface elevation, and total column ozone.

[22] For cloudy sky, we consider the effects of SZA, cloud optical depth (COD), cloud height, cloud phase (water or ice), surface albedo, precipitable water, surface elevation, and total column ozone on adjustment factors γ_7^{dir} and γ_7^{dif} . Figure 6 shows γ_7^{dir} as a function of cosine of SZA for COD of 1 and 5. It decreases as the cosine of the SZA decreases. For larger SZAs and CODs, the direct beam is totally diminished, so the corresponding γ_7^{dir} was not provided in Figure 6. For algorithm application purpose, the value is set to one to avoid numerical overflow. Figure 7 shows γ_7^{dif} as a function of cosine of SZA for different CODs, and we see that like γ_7^{dif} for clear conditions the sensitivity to SZA is relatively modest. The adjustment factor γ_7^{dif} for cloudy skies is somewhat sensitive to surface albedo, but γ_7^{dir} for cloudy skies is not (figures are not shown for economy). Tests reveal that γ_7^{dir} and γ_7^{dif} are not significantly sensitive to cloud height, cloud phase, precipitable water, surface elevation, or total column ozone.

[23] We can calculate surface direct and diffuse PAR if we know adjustment factors γ_7^{dir} , γ_7^{dif} , γ_{10}^{dir} , and γ_{10}^{dif} ,

$$PAR^{dir} = \frac{F_7^{dir}}{\gamma_7^{dir}} + F_8^{dir} + F_9^{dir} + \frac{F_{10}^{dir}}{\gamma_{10}^{dir}}, \quad (1)$$

$$PAR^{dif} = \frac{F_7^{dif}}{\gamma_7^{dif}} + F_8^{dif} + F_9^{dif} + \frac{F_{10}^{dif}}{\gamma_{10}^{dif}}, \quad (2)$$

where PAR^{dir} and PAR^{dif} are the direct and diffuse component of PAR; F_7^{dir} , F_8^{dir} , F_9^{dir} , and F_{10}^{dir} are the direct fluxes for band 7, band 8, band 9, and band 10 from the 15-band SARB SW output; F_7^{dif} , F_8^{dif} , F_9^{dif} , and F_{10}^{dif} are the

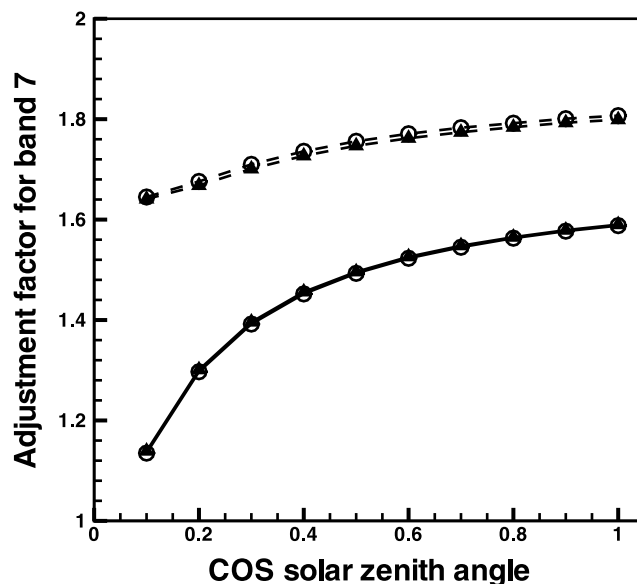


Figure 5. Adjustment factor γ_7^{dir} (solid lines) and γ_7^{dif} (dashed lines) as a function of cosine of SZA for continental average aerosols (triangles) and urban aerosols (circles) with same AOD of 0.2. Sea surface albedo and midlatitude summer atmosphere were used here.

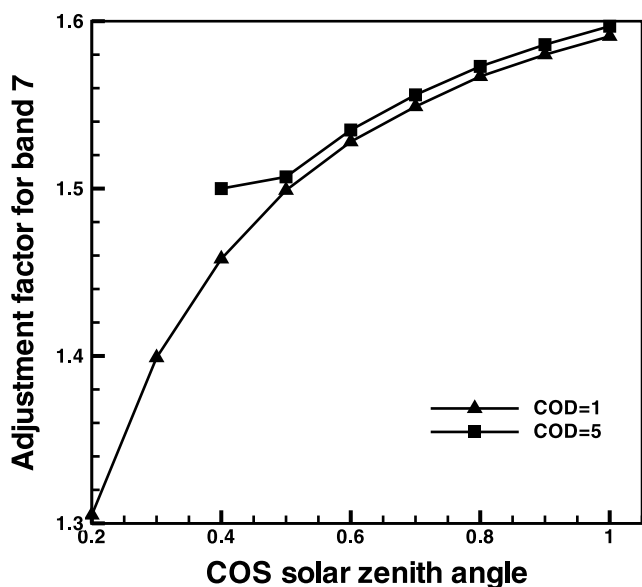


Figure 6. Adjustment factor γ_7^{dir} as a function of cosine of SZA for different COD. Sea surface albedo and midlatitude summer atmosphere were used here.

diffuse fluxes for band 7, band 8, band 9, and band 10. We construct a direct look-up table (LUT) for γ_7^{dir} and γ_{10}^{dir} , and a diffuse LUT for γ_7^{dif} and γ_{10}^{dif} taking into account all the parameters that they are sensitive to. Specifically, the direct LUT includes: (1) cosine of SZA from 0.1 to 1 in steps of 0.1; (2) AOD of 0.02, 0.1, 0.2, 0.5, and 1.0; and (3) COD of 1, 5, 10, 20, 40, 60, 100, 200. Also, the diffuse LUT includes four surface types: ocean, desert, snow, and vegetation, in addition to all the variables in the direct LUT. For a given SARB broadband SW calculation, we use its SZA, AOD, COD, and surface albedo with the direct and diffuse LUT for γ_7^{dir} , γ_7^{dif} , γ_{10}^{dir} , and γ_{10}^{dif} , and then obtain the surface direct PAR and diffuse PAR from equations (1)

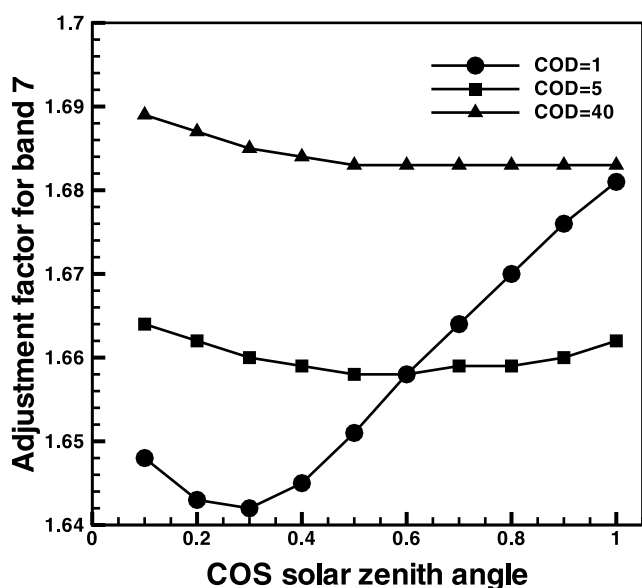


Figure 7. Adjustment factor γ_7^{dif} as a function of cosine of SZA for different COD. Sea surface albedo and midlatitude summer atmosphere were used here.

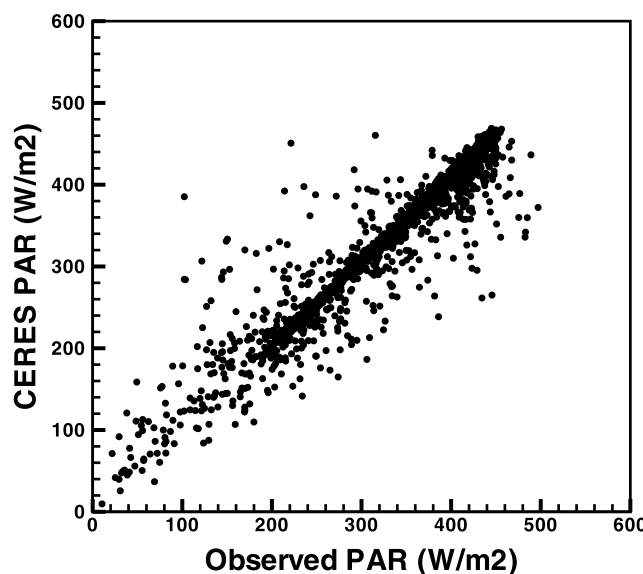


Figure 8. Comparison between SURFRAD observed PAR with CERES retrieved PAR for Desert Rock, Nevada, for all-sky condition, using data from March 2000 to June 2005. The total sample number is 1485, and the bias and RMS error are 4.5 and 35.0 W/m², respectively.

and (2). The surface total PAR is the sum of the direct and diffuse PAR.

[24] As mentioned earlier, some terrestrial ecosystems use the diffuse radiation more efficiently than the direct radiation, so it is important to provide both direct and diffuse PAR components. The advantage of our algorithm is that it calculates the direct and diffuse PAR separately allowing us to provide the direct to diffuse PAR ratio and the total PAR in our CRS and SYNI products.

5. Validation

[25] To evaluate this new technique for PAR retrieval with CERES SARB inputs, we compare results with ground-based LI-COR measurements from the SURFRAD network and ARM SGP CF, and the ratio of direct to diffuse PAR derived from RSS measurements at the ARM SGP CF. The retrieved PAR (400–700 nm) was obtained by rerunning the Terra Edition 2B CRS algorithm for untuned fluxes and then applying the new direct and diffuse look-up tables discussed in section 4.

5.1. Total PAR

[26] SURFRAD was established in 1993 to support climate research with accurate, continuous, and long-term measurements of the surface radiation budget over the United States. Currently seven SURFARD sites are operating in climatologically diverse regions: Fort Peck, Montana; Boulder, Colorado; Bondville, Illinois; Goodwin Creek, Mississippi; Penn State, Pennsylvania; Desert Rock, Nevada; Sioux Falls, South Dakota. The network measures upwelling and downwelling shortwave and longwave broadband fluxes, PAR, erythemal UV, spectral solar, and meteorological parameters. PAR is measured with LI-COR quantum sensor and its uncertainty is estimated to be ±10% (J. Augustine, personal communication, 2006).

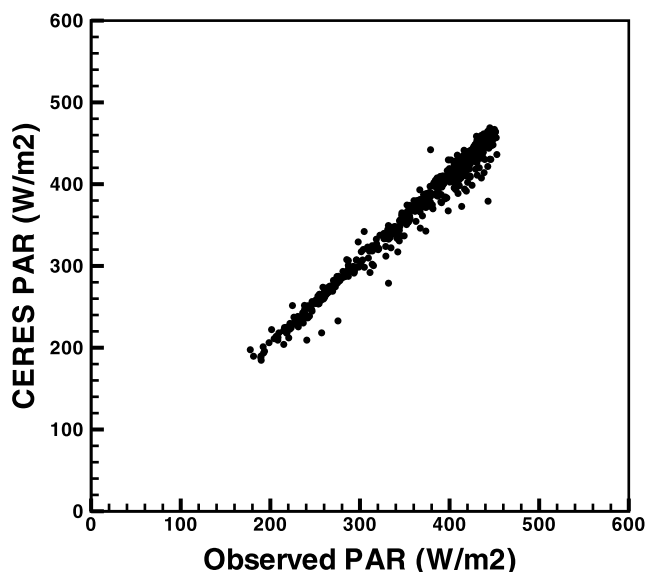


Figure 9. Comparison between SURFRAD observed PAR with CERES retrieved PAR for Desert Rock, Nevada, for clear-sky condition, using data from March 2000 to June 2005. The total sample number is 583, and the bias and RMS error are 6.7 and 13.1 W/m², respectively.

[27] The direct and diffuse LUTs presented in section 4 are applied to CERES on Terra from March of 2000 to June of 2005. Figure 8 shows the observed PAR against CERES PAR for Desert Rock for all-sky conditions. The mean observed PAR is 322.3 W/m², and the mean CERES PAR is 326.8 W/m². The RMS error is 35.0 W/m². Figure 9 is the same as Figure 8, but for clear sky. The mean observed and SARB PAR are 364.7 W/m² and 371.4 W/m², and the RMS error is reduced to 13.1 W/m² for clear-sky conditions. The all-sky RMS (35.0 W/m²) is much larger because clouds in the large CERES field of view (about 20 km at nadir) often differ from those immediately above the ground radiometer. Clear conditions in Figure 9 were identified with MODIS pixels within the CERES footprint. If MODIS misses a cloud and marks a footprint as clear, the signal would be cases of observed PAR falling much below the retrieved PAR; a few of these are seen in Figure 9. Table 1 provides the total sample number, mean observed PAR, mean CERES PAR, Root Mean Square (RMS) error, bias (CERES minus

observed), and relative bias (bias/observed*100%) for the seven SURFRAD sites for all-sky and clear-sky conditions. PAR retrieved from CERES is higher than the SURFRAD measurements, except for Fort Peck under clear sky. Bondville has the largest relative bias for both all sky (9.3%) and clear sky (6.7%). Desert Rock has the lowest relative bias for all sky (1.4%) and Fort Peck has the lowest relative bias for clear sky (−0.1%).

[28] Snow and ice surfaces are the most challenging targets for satellite retrievals of SW flux at the surface. To test the performance of the algorithm over snow/ice surface, we use broadband surface albedo observed at the SURFRAD sites to distinguish low surface albedo (<0.6) and high surface albedo (≥0.6) samples. We further divide all-sky and clear-sky samples into low- and high-albedo categories. Results for Fort Peck, presented in Table 2, show the algorithm overestimates PAR for all-sky conditions and slightly underestimates PAR for clear-sky conditions for both low- and high-albedo surfaces. Results from five sites having both low and high surface albedo records show that the biases are comparable for low and high albedos.

[29] How many of PAR retrievals fall within the specified uncertainty of the LI-COR quantum sensor? We calculate the relative difference of PAR as observed minus CERES then divided by observed. We define the percentage of samples with relative difference between a% and b% as

$$P_{a\% \sim b\%} = \frac{1}{N} \sum_{i=1}^N \delta_i \times 100\% \quad \begin{cases} \delta_{i=1} & a\% < R_i \leq b\% \\ \delta_{i=0} & R_i \leq a\% \text{ or } R_i > b\% \end{cases} \quad (3)$$

where R_i is the relative difference of the i th sample, and N is the total number of samples. Figure 10 shows the sample percentage distribution in 12 relative difference bins at Desert Rock for all-sky (solid line) and clear-sky (dashed line) conditions. For all sky, 80% of the samples (1188 out of 1485) have relative differences within ±10%; for clear-sky condition, 98% of the samples (571 out of 583) have relative differences within ±10%. The percentage of samples with relative difference between −10% and +10% ($P_{-10\% \sim +10\%}$) are shown in the last row of Table 1. For all sky, Penn State has the lowest percentage of samples (40%) with relative difference within ±10%, and Desert Rock has the highest percentage (80%). For clear sky, Bondville has the lowest percentage of samples (72%) with

Table 1. Total Sample Number, Mean Observed PAR, Mean CERES PAR, RMS Error, Bias, Relative Bias, and Percentage of Samples With Relative Difference Within ±10% for the Seven SURFRAD Sites for All-Sky and Clear-Sky Conditions^a

	Bondville		Boulder		Desert Rock		Fort Peck		Goodwin Creek		Penn State		Sioux Falls	
	All	Clear	All	Clear	All	Clear	All	Clear	All	Clear	All	Clear	All	Clear
Number	1076	371	1648	199	1485	583	1901	457	1497	300	1676	200	650	166
Mean observed PAR	223.7	292.4	267.2	299.7	322.3	364.7	224.2	272.2	244.9	304.9	204.6	299.6	232.2	293.5
Mean CERES	244.4	312.2	275.8	304.6	326.8	371.4	229.1	271.6	262.7	318.0	216.6	314.8	241.7	301.0
RMS	51.0	40.6	63.4	18.0	35.0	13.1	41.0	16.1	49.1	17.5	52.0	37.5	42.4	18.7
Bias	20.8	19.8	8.6	4.9	4.5	6.7	4.9	−0.5	17.8	13.1	12.1	15.2	9.4	7.6
Relative bias	9.3	6.7	3.2	1.6	1.4	1.8	2.2	−0.1	7.2	4.3	5.9	5.1	4.0	2.6
$P_{-10\% \sim +10\%}$	45	72	53	97	80	98	55	87	53	97	40	80	54	92

^aPAR and RMS error are in W/m². Bias is CERES minus observed in W/m², and relative bias is bias/observed × 100%.

Table 2. Total Sample Number, Mean Observed PAR, Mean CERES PAR, RMS Error, Bias, and Relative Bias at Fort Peck for Low-Albedo (<0.6) and High-Albedo (≥ 0.6) Surfaces Under All-Sky and Clear-Sky Conditions^a

	All		Clear	
	Low	High	Low	High
Number	1582	319	364	93
Mean Obs	236.8	161.5	294.6	184.3
Mean CERES	241.8	166.3	294.4	182.6
RMS	41.5	38.2	15.3	18.9
Bias	5.0	4.8	-0.2	-1.7
Relative Bias	2.1	3.0	-0.1	-0.9

^aPAR and RMS error are in W/m^2 . Bias is CERES minus observed in W/m^2 , and relative bias is bias/observed $\times 100\%$.

relative difference within $\pm 10\%$, and Desert Rock has the highest percentage (98%). Over the course of more than five years, there are over 10,000 validation samples from the seven SURFRAD sites, with 54% within the PAR measurement uncertainty. Over 2200 samples are taken under clear sky, and 89% of the clear-sky samples are within the PAR measurement uncertainty. At all sites, the relative biases of the respective 5-year ensemble mean retrievals are less than 10%, for both all-sky and clear-sky conditions.

[30] It is useful to compare the discrepancies of retrievals and observations for surface PAR with those for surface broadband SW. We present such a comparison for all the data available from the seven SURFRAD sites in Table 3. The relative biases (bias divided by the observed) for PAR retrievals are 4.6% for all sky and 2.9% for clear sky, and the relative biases for broadband SW retrievals are 0.8% for all sky and 0.7% for clear sky. The surface downwelling SW fluxes derived from CERES agree with the observations much better than the PAR from CERES with observations. This is not surprising because the LI-COR sensor's uncertainty (10%) is much larger than that of the SW pyranometer. SURFRAD [Augustine *et al.*, 2000] broadband measurements adhere to the strict observing and calibration protocol of the Baseline Surface Radiation Network [Ohmura *et al.*, 1998]. The large sample (10,563 for all-sky) ensures that the relative biases for the PAR (4.6%) and broadband SW (0.8%) are statistically significant. For an instantaneous FOV however, the discrepancy of the satellite and ground-based PAR is about the same as the discrepancy of the satellite and ground-based broadband SW: the relative PAR RMS error (RMS divided by observed in Table 3) is 20% for all sky, versus the relative broadband SW RMS error of 19% for all sky. The RMS is mostly a marker of the space-time discrepancy between the satellite FOV (~ 20 – 40 km) and ground-based measurement at a point (here 15-min averages). The spatial variation of cloud properties over a typical instantaneous FOV accounts for the bulk of the RMS signal in all-sky conditions.

[31] Given the substantial uncertainty quoted for the LI-COR PAR sensor, we use the more accurate RSS instrument at ARM SGP CF for additional tests. We integrate the total spectral fluxes of RSS from 400 nm to 700 nm to produce the total PAR at CF site. There is also a LI-COR PAR sensor, which is maintained by the USDA at the CF. We use data from October 2003 to June 2004 to compare the

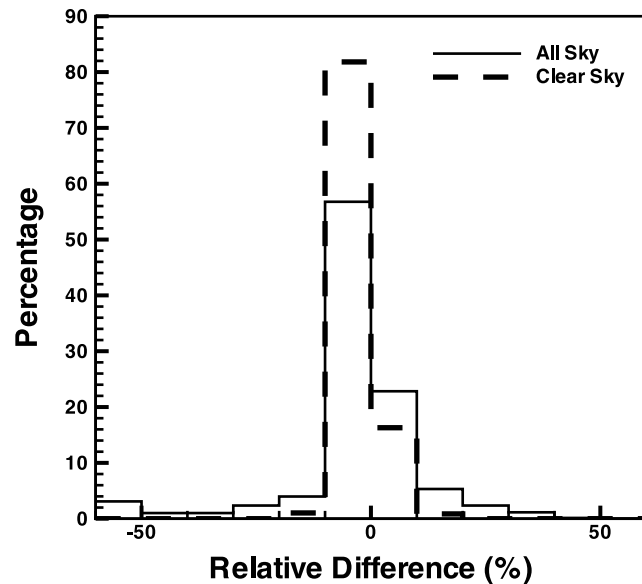


Figure 10. Sample percentage distribution for 12 relative difference bins for Desert Rock under all-sky (solid line) and clear-sky (dashed line) conditions.

CERES PAR with PAR from LI-COR sensor and RSS (Figure 11). The total sample numbers are 136. The mean RSS integrated PAR is $245.8 W/m^2$, and the mean LI-COR PAR is $231.0 W/m^2$. The mean CERES PAR is $235.5 W/m^2$, which falls in between. Linear regression between CERES PAR and RSS PAR (LI-COR PAR) yields the slope of 1.03 (0.95) and regression coefficient of 0.93 (0.94). Table 4 provides the RMS errors and biases between CERES PAR and LI-COR PAR, between CERES PAR and RSS PAR, and between RSS PAR and LI-COR PAR. The mean CERES surface downwelling SW flux and the mean pyranometer observed downwelling SW flux, and the RMS error and bias between them are also included in Table 4. Here the CERES PAR agrees slightly better with the LI-COR PAR sensor. Comparing to PAR measurements, the SW measurements have a smaller relative RMS discrepancies and relative biases with CERES retrievals for both all-sky and clear-sky conditions, which manifests the results

Table 3. Total Sample Number, Mean Observed, Mean CERES, RMS Error, Bias, and Relative Bias for PAR (400–700 nm) and SW (Broadband) Derived at Seven SURFRAD Sites^a

	All Sky	Clear Sky
Number	10563	2278
Mean LI-COR observed PAR	244.9	309.9
Mean CERES PAR	256.2	318.8
PAR RMS	49.1	24.1
PAR Bias	11.3	8.9
Relative PAR bias	4.6	2.9
Mean observed SW	571.7	732.1
Mean CERES SW	576.4	726.7
SW RMS	107.8	29.8
SW Bias	4.7	-5.4
Relative SW bias	0.8	0.7

^aMean observed, mean CERES, and RMS error are in W/m^2 . Bias is CERES minus observed in W/m^2 , and relative bias is bias/observed $\times 100\%$.

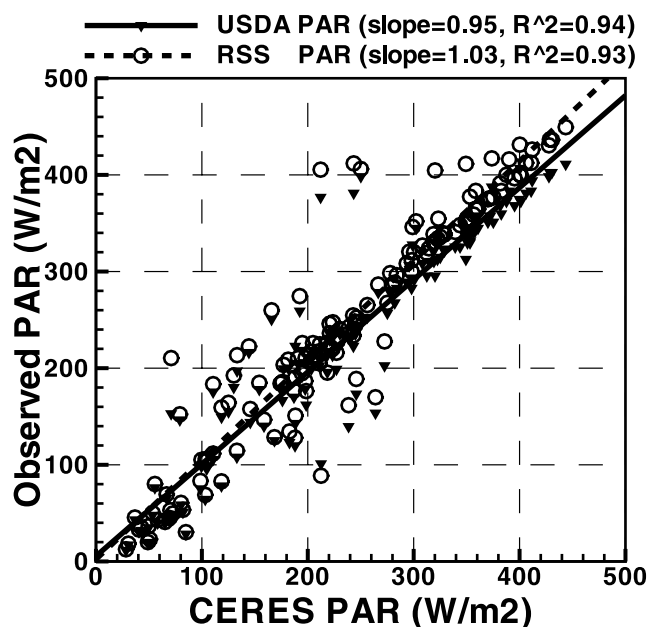


Figure 11. Comparison between CERES PAR to RSS integrated PAR (open circles) and Licor PAR (solid gradients) at ARM SGP site. The slope between CERES PAR and RSS integrated PAR is 1.03 (dashed line) and correlation coefficient is 0.93, and the slope between CERES PAR and Licor PAR is 0.95 (solid line) and the correlation coefficient is 0.94.

from SURFRAD sites. We also note the relative bias for PAR at the Central Facility is smaller than that at the SURFRAD sites (see Table 3). Nevertheless, the errors between CERES retrieved PAR and the observed PAR are all within each instrument's uncertainty. Therefore significant improvement in the validation of the satellite retrieved PAR product for total horizontal flux (rather than the ratio of separate direct to diffuse components of PAR, as in the next section) will rely on the availability of more accurate surface PAR instrumentation.

5.2. Direct and Diffuse PAR

[32] We also derive the ratio of direct to diffuse PAR at SGP CF from the total and diffuse spectral fluxes of RSS. Here we use data from July 2003 to June 2004. Figure 12 compares the ratios of direct to diffuse PAR derived from RSS with those from SARB for clear and cloudy conditions. The total sample numbers are 270. The mean ratios are 2.59 and 1.93 from RSS and CERES with an RMS error of 1.40. CERES SARB underestimates the direct to diffuse PAR ratio, but the relative error of the retrieved ratio for clear conditions is much less than for cloudy conditions. The large error for the retrieved ratio in cloudy skies is mostly due to a fundamental mismatch of the retrieval (a calculation) and observation in the spatial and temporal domains. There is only one mean ratio for a given CERES FOV (~ 20 – 30 km in length), and it is based on a maximum of just three instantaneous radiative transfer calculations, potentially covering a clear portion, a first cloudy portion, and a second cloudy portion. The observed ratio is the 15-min

mean of the direct flux (which can be large to near zero) to the 15-min mean of the diffuse flux (which is less than the direct flux for a clear sky). The observation itself represents a small area, perhaps just a few square kilometers, when cloudy. Because the optical properties of clouds are usually inhomogeneous, the ratio for one cloudy square km can differ greatly from those in nearby cloudy squares. Since the retrieved ratio represents such a large area, and is hence generally smaller than the observed ratio. This space-time mismatch accounts for most of the bias in the retrieved ratio. Other factors, such as 3-D effect of clouds, are secondary.

6. Summary and Discussion

[33] The Surface and Atmospheric Radiation Budget (SARB) product uses retrieved aerosol and cloud optical properties from the collocated imagers, and aerosol assimilation model to calculate the vertical flux profiles of shortwave, longwave, and window channels. To fully exploit the capability of SARB product, we develop look-up tables to adjust the spectrum discrepancies of its band 7 (357.5–437.4 nm) and band 10 (595.5–689.7 nm) from PAR spectral range: namely adjust band 7 to spectral range (400–437.5 nm) and band 10 to spectral range (595.5–700 nm). The adjustment is done separately for direct and diffuse fluxes; therefore we provide the ratio of direct to diffuse PAR, in addition to the total PAR. These look-up tables are applied to five-year CERES Terra data and the retrieved surface PAR is validated against SURFRAD measured PAR. Our algorithm overestimates surface PAR for both all-sky and clear-sky conditions, except for Fort Peck under clear-sky condition. Relative bias ranges from 1.4% to 9.3% for all sky, and from -0.1% to 6.7% for clear sky. For high-reflecting surface, the algorithm underestimates the surface PAR at Bondville, Penn State, and Sioux

Table 4. Total Sample Number, Mean LI-COR Observed PAR, Mean CERES PAR, Mean RSS Observed PAR, and the RMS Errors, Biases, and Relative Biases of Each Pair^a

	All Sky	Clear Sky
Number	136	51
Mean LI-COR observed PAR	231.0	293.7
Mean CERES PAR	235.5	301.4
PAR RMS CERES/LI-COR	38.6	17.8
PAR Bias CERES/LI-COR	4.5	7.7
Relative PAR bias CERES/LI-COR	1.9	2.6
Mean RSS observed PAR	245.8	309.6
PAR RMS CERES/RSS	42.1	14.6
PAR Bias CERES/RSS	-10.3	-8.2
Relative PAR bias CERES/LI-COR	-4.2	-2.6
RMS LI-COR/RSS	21.4	18.1
Bias LI-COR/RSS	-14.8	-15.9
Relative bias	8.7	5.1
Mean observed SW	526.0	686.0
Mean CERES SW	531.6	679.3
SW RMS	63.2	24.0
SW Bias	5.6	6.7
Relative SW bias	1.1	1.0

^aThe bottom five rows are the mean observed broadband SW (W/m^2), mean CERES broadband SW (W/m^2), RMS error (W/m^2), bias (W/m^2), and relative bias (%) for the ARM SGP Central Facility. PAR and RMS error are in W/m^2 . Bias is CERES minus observed in W/m^2 , and relative bias is bias/observed $\times 100\%$ in %.

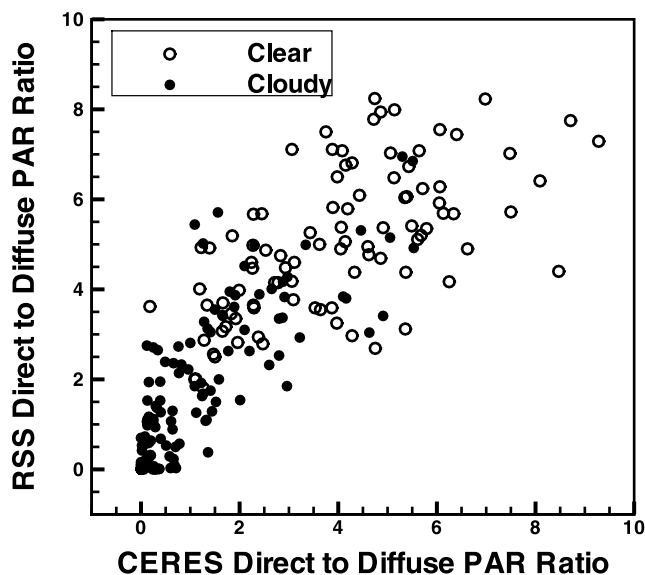


Figure 12. Comparison between ratio of direct PAR to diffuse PAR derived from RSS and CERES at ARM SGP site for clear (open circles) and cloudy (solid circles) conditions.

Falls. Nevertheless, the absolute relative biases are comparable for both low- and high-reflecting surfaces. Therefore we conclude that the algorithm works equally well for snow and ice surface. We use more than 10,000 samples from SURFRAD measurements to validate the PAR product, and 54% of these samples are within the $\pm 10\%$ uncertainty of PAR measurements. There are over 2200 clear-sky samples, and 89% of them are within the uncertainty of PAR measurements. Rotating Shadowband Spectroradiometer (RSS) has been used to validate the ratio of direct to diffuse PAR at ARM SGP site. The mean ratio derived from CERES SARB is 1.93 and the mean ratio from RSS is 2.59. Our algorithm underestimates the ratio for both clear and cloudy conditions.

[34] Finally, the three-hourly SYNI PAR product can alternatively be used as the input to the MODIS net primary production model. Also the ratio of direct to diffuse PAR that is available from CERES SYNI product can help to quantify the enhancement of terrestrial carbon uptake by increased proportion of diffuse PAR.

[35] **Acknowledgments.** We would like to thank John Augustine from SURFRAD and James Slusser from USDA UV network for providing data used in this study. ARM data is made available through the U.S. Department of Energy as part of the Atmospheric Radiation Measurement program. Wenying Su is supported by the CERES project under NASA grant NNL04AA26G.

References

- Arduini, R. F., P. Minnis, and D. F. Young (2002), Investigation of a visible reflectance parameterization for determining cloud properties in multi-layered clouds, paper presented at 11th Conference on Cloud Physics, Am. Meteorol. Soc., Boston, Mass.
- Augustine, J. A., J. J. DeLuise, and C. N. Long (2000), SURFRAD—A national surface radiation budget network for atmospheric research, *Bull. Am. Meteorol. Soc.*, *81*, 2341–2357.
- Baldocchi, D., et al. (2001), FLUXNET: A new tool to study the temporal and spatial variability of ecosystem-scale carbon dioxide, water vapor, and energy flux densities, *Bull. Am. Meteorol. Soc.*, *82*, 2415–2434.
- Bigelow, D. S., J. R. Slusser, A. F. Beaubien, and J. H. Gibson (1998), The USDA ultraviolet radiation monitoring program, *Bull. Am. Meteorol. Soc.*, *79*, 601–615.
- Bishop, J. K. B., and W. B. Rossow (1991), Spatial and temporal variability of global surface solar irradiance, *J. Geophys. Res.*, *96*, 16,839–16,858.
- Bishop, J. K. B., W. B. Rossow, and E. G. Dutton (1997), Surface solar irradiance from the International Satellite Cloud Climatology Project 1983–1991, *J. Geophys. Res.*, *102*, 6883–6910.
- Bloom, S., et al. (2005), Documentation and validation of the Goddard Earth Observing System (GEOS) data assimilation system, version 4, *Tech. Rep. 104606*, NASA Goddard Space Flight Cent., Greenbelt, Md.
- Charlock, T. P., and T. L. Alberta (1996), The CERES/ARM/GEWEX experiment (CAGEX) for the retrieval of radiative fluxes with satellite data, *Bull. Am. Meteorol. Soc.*, *77*, 2673–2683.
- Charlock, T. P., F. G. Rose, D. A. Rutan, Z. Jin, and S. Kato (2006), The global surface and atmosphere radiation budget: An assessment of accuracy with 5 years of calculations and observations, paper presented at 12th Conference on Atmospheric Radiation, Am. Meteorol. Soc., Boston, Mass.
- Cohan, D. S., J. Xu, R. Greenwald, M. H. Bergin, and W. L. Chameides (2002), Impact of atmospheric aerosol light scattering and absorption on terrestrial net primary productivity, *Global Biogeochem. Cycles*, *16*(4), 1090, doi:10.1029/2001GB001441.
- Collins, W. D., P. J. Rasch, B. E. Eaton, B. V. Khattatov, J.-F. Lamarque, and C. S. Zender (2001), Simulating aerosols using a chemical transport model with assimilation of satellite aerosol retrievals: Methodology for INDOEX, *J. Geophys. Res.*, *106*, 7313–7336.
- d’Almeida, G. A., P. Koepke, and E. P. Shettle (1991), *Atmospheric Aerosols—Global climatology and radiative characteristics*, A. Deepak, Hampton, VA.
- Dye, D. G., and R. Shibasaki (1995), Intercomparison of global PAR data sets, *Geophys. Res. Lett.*, *22*, 2013–2016.
- Eck, T., and D. G. Dye (1991), Satellite estimation of incident photosynthetically active radiation using ultraviolet reflectance, *Remote Sens. Environ.*, *38*, 135–146.
- Fan, S. M., M. L. Goulden, J. W. Munger, B. C. Daube, P. S. Bakwin, S. C. Wofsy, J. S. Amthor, D. R. Fitzjarrald, K. E. Moore, and T. R. Moore (1995), Environmental controls on the photosynthesis and respiration of a boreal lichen woodland: A growing season of whole-ecosystem exchange measurements by eddy correlation, *Oecologia*, *102*, 443–452.
- Frouin, R., B. A. Franz, and P. J. Werdell (2003), The SeaWiFS PAR product, in *Algorithm Updates for the Fourth SeaWiFS Data Reprocessing*, NASA Tech. Memo., 2003–206892, 22, 46–50.
- Fu, Q., and K.-N. Liou (1992), On the correlated-k distribution method for radiative transfer in nonhomogeneous atmospheres, *J. Atmos. Sci.*, *49*, 2139–2156.
- Fu, Q., and K.-N. Liou (1993), Parameterization of the radiative properties of cirrus clouds, *J. Atmos. Sci.*, *50*, 2008–2025.
- Goulden, M. L., B. C. Daube, S. M. Fan, D. J. Sutton, A. Bazzaz, J. W. Munger, and S. C. Wofsy (1997), Physiological responses of a black spruce forest to weather, *J. Geophys. Res.*, *102*, 28,987–28,996.
- Gu, L., J. D. Fuentes, H. H. Shugart, R. M. Staebler, and T. A. Black (1999), Response of net ecosystem exchanges of carbon dioxide to changes in cloudiness: Results from two North American deciduous forests, *J. Geophys. Res.*, *104*, 31,421–31,434.
- Gu, L., D. Baldocchi, S. B. Verma, T. A. Black, T. Vesala, E. M. Falge, and P. R. Dwyty (2002), Advantages of diffuse radiation for terrestrial ecosystem productivity, *J. Geophys. Res.*, *107*(D6), 4050, doi:10.1029/2001JD001242.
- Harrison, L., M. Beauharnois, J. Berndt, P. Kiedron, J. Michalsky, and Q. Min (1999), The rotating shadowband spectroradiometer (RSS) at SGP, *Geophys. Res. Lett.*, *26*, 1715–1718.
- Harrison, L., P. Kiedron, J. Berndt, and J. Schlemmer (2003), Extraterrestrial solar spectrum 360–1050 nm from rotating shadowband spectroradiometer measurements at the Southern Great Plains (ARM) site, *J. Geophys. Res.*, *108*(D14), 4424, doi:10.1029/2001JD001311.
- Hess, M., P. Koepke, and I. Schult (1998), Optical properties of aerosols and clouds: The software package OPAC, *Bull. Am. Meteorol. Soc.*, *79*, 831–844.
- Hollinger, D. Y., F. M. Kelliher, J. N. Byers, J. E. Hunt, T. M. McSeveny, and P. L. Weir (1994), Carbon dioxide exchange between an undisturbed old-growth temperate forest and the atmosphere, *Ecology*, *75*, 134–150.
- Ignatov, A., and L. Stowe (2000), Physical basis, premises, and self-consistency checks of aerosol retrievals from TRMM VIRS, *J. Appl. Meteorol.*, *39*, 2259–2277.
- Jin, Z., and K. Stamnes (1994), Radiative transfer in nonuniformly refracting layered media: Atmosphere-ocean system, *Appl. Opt.*, *33*, 431–442.
- Jin, Z., T. P. Charlock, W. L. Smith Jr., and K. Rutledge (2004), A parameterization of ocean surface albedo, *Geophys. Res. Lett.*, *31*, L22301, doi:10.1029/2004GL021180.

- Kato, S., T. Ackerman, J. Mather, and E. Clothiaux (1999), The k-distribution method and correlated-k approximation for a shortwave radiative transfer model, *J. Quant. Spectrosc. Radiat. Transfer*, *62*, 109–121.
- Kato, S., F. G. Rose, and T. P. Charlock (2005), Computation of domain-averaged irradiance using satellite-derived cloud properties, *J. Atmos. Oceanic Technol.*, *22*, 146–164.
- Kaufman, Y. J., D. Tanre, L. A. Remer, E. F. Vermote, and A. Chu (1997), Operational remote sensing of tropospheric aerosol over land from EOS moderate resolution imaging spectroradiometer, *J. Geophys. Res.*, *102*, 17,051–17,061.
- Kiedron, P. W., J. J. Michalsky, J. L. Berndt, and L. Harrison (1999), Comparison of spectral irradiance standards used to calibrate shortwave radiometers and spectroradiometers, *Appl. Opt.*, *38*, 2432–2439.
- Minnis, P., et al. (2002), Seasonal and diurnal variations of cloud properties derived for CERES from VIRS and MODIS data, paper presented at 11th Conference on Atmospheric Radiation, Am. Meteorol. Soc., Boston, Mass.
- Niyogi, D., et al. (2004), Direct observations of the effects of aerosol loading on net ecosystem CO₂ exchanges over different landscapes, *Geophys. Res. Lett.*, *31*, L20506, doi:10.1029/2004GL020915.
- Ohmura, A., et al. (1998), Baseline surface radiation network (BSRN/WCRP): New precision radiometry for climate research, *Bull. Am. Meteorol. Soc.*, *79*, 2115–2136.
- Pinker, R. T., and J. A. Ewing (1985), Modeling surface solar radiation: Model formulation and validation, *J. Clim. Appl. Meteorol.*, *24*, 389–401.
- Pinker, R. T., and I. Laszlo (1992a), Global distribution of photosynthetically active radiation as observed from satellites, *J. Clim.*, *5*, 56–65.
- Pinker, R. T., and I. Laszlo (1992b), Modeling surface solar irradiance for satellite applications on global scale, *J. Appl. Meteorol.*, *31*, 194–211.
- Platnick, S., J. Y. Li, M. D. King, H. Gerber, and P. V. Hobbs (2001), A solar reflectance method for retrieving cloud optical thickness and droplet size over snow and ice surfaces, *J. Geophys. Res.*, *106*, 15,185–15,199.
- Potter, C. S., J. T. Randerson, C. B. Field, P. A. Matson, P. M. Vitousek, H. A. Mooney, and S. A. Klooster (1993), Terrestrial ecosystem production: A process model based on global satellite and surface data, *Global Biogeochem. Cycles*, *7*, 811–841.
- Price, D. T., and T. A. Black (1990), Effects of short-term variation in weather on diurnal canopy CO₂ flux and evapotranspiration of a juvenile douglas-fir stand, *Agric. For. Meteorol.*, *50*, 139–158.
- Rabier, F., J.-N. Thepaut, and P. Courtier (1998), Extended assimilation and forecast experiments with a four-dimensional variational assimilation, *Q. J. R. Meteorol. Soc.*, *124*, 1861–1887.
- Ricchiazzi, P., S. Yang, C. Gautier, and D. Sowle (1998), SBDART: A research and teaching software tool for plane-parallel radiative transfer in the earth's atmosphere a research and teaching software tool for plane-parallel radiative transfer in the Earth's atmosphere, *Bull. Am. Meteorol. Soc.*, *79*, 2101–2114.
- Rose, F. G., and T. P. Charlock (2002), New fu-liou code tested with ARM raman lidar and CERES in pre-CALIPSO exercise, paper presented at 11th Conference on Atmospheric Radiation, Am. Meteorol. Soc., Boston, Mass.
- Rose, F. G., T. P. Charlock, B. A. Wielicki, D. Doelling, and S. Zentz (2006), CERES synoptic gridded diurnally averaged radiative transfer, paper presented at 12th Conference on Atmospheric Radiation, Am. Meteorol. Soc., Boston, Mass.
- Rossow, W. B., and R. A. Schiffer (1991), ISCCP cloud data products, *Bull. Am. Meteorol. Soc.*, *72*, 2–20.
- Running, S. W., R. R. Nemani, F. A. Heinsch, M. Zhao, M. Reeves, and H. Hashimoto (2004), A continuous satellite-derived measure of global terrestrial primary production, *BioScience*, *54*, 547–560.
- Rutan, D. A., T. P. Charlock, F. G. Rose, S. Kato, S. Zentz, and L. Coleman (2006), Global surface albedo from CERES/TERRA surface and atmospheric radiation budget (SARB) data product, paper presented at 12th Conference on Atmospheric Radiation, Am. Meteorol. Soc., Boston, Mass.
- Su, W., T. P. Charlock, and F. G. Rose (2005), Deriving surface ultraviolet radiation from CERES surface and atmospheric radiation budget: Methodology, *J. Geophys. Res.*, *110*, D14209, doi:10.1029/2005JD005794.
- Tegen, I., and A. A. Lacis (1996), Modeling of particle size distribution and its influence on the radiative properties of mineral dust aerosol, *J. Geophys. Res.*, *101*, 19,237–19,244.
- Wielicki, B. A., B. R. Barkstrom, E. F. Harrison, R. B. Lee, G. L. Smith, and J. E. Cooper (1996), Clouds and the Earth's radiant energy system (CERES): An Earth observing system experiment, *Bull. Am. Meteorol. Soc.*, *77*, 853–868.
- Young, D. F., P. Minnis, D. R. Doelling, G. G. Gibson, and T. Wong (1998), Temporal interpolation methods for the clouds and the Earth's radiant energy system (CERES) experiment, *J. Appl. Meteorol.*, *37*, 572–590.

T. P. Charlock, NASA Langley Research Center, Hampton, VA 23681, USA. (thomas.p.charlock@nasa.gov)

F. G. Rose, D. Rutan, and W. Su, Science Systems and Applications, Inc., 1 Enterprise Parkway, Hampton, VA 23666, USA. (f.g.rose@larc.nasa.gov; d.a.rutan@larc.nasa.gov; w.su@larc.nasa.gov)